PHYSICAL REVIEW A VOLUME 24, NUMBER 2 AUGUST 1981

Two-step polarization-labeling spectroscopy of excited states of Na_2

N. W. Carlson,* A. J. Taylor, K. M. Jones, and A. L. Schawlow
Department of Physics, Stanford University, Stanford, California 94305
(Received 10 February 1981)

Two-step polarization-labeling spectroscopy of diatomic molecules is described. Formulas for relative transition intensities are derived, and their use in determining angular momenta of molecular states is discussed. The experimental apparatus and procedure used to identify twenty-four new $^1\Sigma_g^+$, $^1\Pi_g$, and $^1\Delta_g$ states in Na_2 are described. The states are identified as low-lying members, $n = 3$ to 14, of several molecular Rydberg series, and the dependence of their properties on principal quantum numbers is shown. These results are extrapolated to yield constants for the ground state of Na_2^+.

I. INTRODUCTION

Laser labeling techniques[1-3] provide powerful ways to study the excited states of molecules. They yield simplified spectra, since only transitions from a chosen vibrational-rotational level are seen. Conventional absorption and emission spectroscopy, on the other hand, provide very complicated spectra, showing transitions from all thermally populated levels. Another advantage of the labeling methods is that one can simply and unambiguously determine the angular momentum of the excited state. Polarization labeling especially makes possible wide-ranging searches for and identification of states. This paper will deal with the theoretical and experimental aspects of polarization labeling in diatomic molecules.

Polarization labeling[2] uses a polarized, narrow-band laser, tuned to resonance with a molecular transition, to populate differentially the degenerate angular-momentum sublevels of the upper state and differentially deplete those of the lower state, producing an optical anisotropy in the upper and lower levels of the pumped transition. If a linearly polarized probe laser is tuned to be resonant with a molecular transition involving either pumped level, it can undergo a change in polarization. The polarization of a broad-band probe beam will be altered only at those frequencies resonant with a transition which has a common level with the pumped transition. If the probe beam is passed through a crossed polarizer and then into a spectrometer, those frequencies will appear as a bright line spectrum and can be recorded photographically. The spectrum is greatly simplified since only transitions from the upper and lower levels of the pumped transition are observed. From the types of signals observed one can determine Λ for the state. In two-step-polarization labeling, the pump laser produces oriented molecules in a low-lying excited electronic state, and the probe reveals transitions to even more highly excited states.

We have used the technique of two-step-polarization labeling to study excited *gerade* states in Na_2.[3-5] The resulting simplified spectra have made it possible to study 24 new excited states whose energies lie between 28 328 and 38 908 cm^{-1}. For each state we have determined Λ, as well as rotational and vibrational constants. The $^1\Delta_g$ states that we have seen are the low-lying members of a molecular Rydberg series, while the $^1\Pi_g$ states span the transition from molecular states to Rydberg states. Both the $^1\Delta_g$ series and the $^1\Pi_g$ series correspond to $3s + nd$ asymptotes. We discuss the dependence of the properties of Na_2 on the principal quantum number n of the excited states. From the behavior of these states at large values of n, we are able to determine the rotational and vibrational constants, as well as the dissociation energy of the ground state of Na_2^+.

Other two-photon techniques have been used to study excited states in diatomic molecules. Woerdman[6] first observed Doppler-free two-photon signals in Na_2. Vasuedev *et al.*[7] have used the ELLIPSA experimental technique to identify excited states in Na_2. Bernheim *et al.*[8,9] have used optical-optical double resonance to identify and characterize several excited states in Li_2.

II. THEORY

Two-step polarization labeling uses probe transitions from the upper level of the pumped transition to examine higher excited states. In this section we calculate the dependence of the intensities of the probe signals on the total angular momentum along the internuclear axes Λ, Λ_1, and Λ_2 (see Fig. 1) for both a circularly polarized pump beam and for one linearly polarized at 45° with respect to the probe beam. We then specialize to the case of a homonuclear diatomic molecule with a $^1\Sigma_g^+$ ground state, where the upper level of the two-step process must be $^1\Sigma_g$, $^1\Pi_g$, or $^1\Delta_g$, and show how to classify an excited state from its polarization spectra.

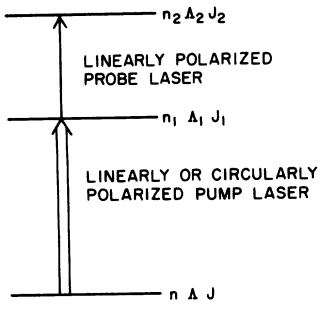

FIG. 1. Schematic of two-step polarization labeling.

Consider the case where the pump beam is circularly polarized. The induced optical anisotropy causes the absorption coefficients and indices of refraction to be different for right and left circularly polarized light interacting with either of the levels of the pumped transition. A linearly polarized probe can be represented as a superposition of two equal components of right- and left-circular polarizations. The difference in indices of refraction causes a small rotation of the pump's polarization, while the difference in absorption coefficients results in a small ellipticity of the probe polarization.

In a typical polarization-labeling experiment, the absorption and saturation of the probe are small and the analyzer is nearly orthogonal to the probe's polarization. Under these conditions the intensity of the probe signal on line center is given by[10,11]

$$I = I_0[\gamma + (\tfrac{1}{4}\Delta\alpha l)^2]\,. \tag{1}$$

In this relation, I_0 is the probe intensity before the medium, γ is a background term due to the finite extinction ratio of the polarizers, the uncrossing of the analyzer, and the background birefringence, and l is the length of the absorption path. For a circularly polarized pump beam, $\Delta\alpha = \alpha^+ - \alpha^-$ is the difference in absorption coefficients between right- and left-circular polarizations. It is assumed here that the background birefringence b and the uncrossing angle of the analyzer θ are both small, such that both $b \ll \Delta\alpha l$ and $\theta \ll \Delta\alpha l$ hold. Both of these conditions can be satisfied in the laboratory. In a Doppler-limited polarization-labeling experiment where the spectra are recorded photographically, the details of the line shape are unimportant, and it is only necessary to consider the intensity when the probe is tuned to the center of the transition.

In order to evaluate the angular-momentum dependence of the signal intensities, we must calculate $\Delta\alpha$. A schematic diagram of the two-step process is shown in Fig. 1. The calculation of $\Delta\alpha$ will follow the rate-equation model of Refs. 5 and 11. In this calculation the following assumptions are made:

(1) The molecules are at rest. (Including a broad velocity distribution, and averaging over this distribution, just brings a factor of order unity to many of the equations.)

(2) The pulse length of the pump laser is shorter than or equal to the lifetimes of the levels of the pumped transition.

(3) The lower level of the pumped transition is not significantly repopulated by fluorescence.

These conditions are satisfied for pulsed dye-laser spectroscopy of many diatomic molecules. Using the above assumptions in a rate-equation model, a circularly polarized pump laser populates the degenerate angular-momentum sublevels (M levels) of the upper level of the pumped transition according to

$$n_{M_1} = \frac{N_0}{2J+1}\sum_M \sigma^{\pm}_{JMJ_1M_1}\left(\frac{It}{\hbar\omega}\right)\left[1+\left(\frac{2\tau I\sigma^{\pm}_{JMJ_1M_1}}{\hbar\omega}\right)^2\right]^{-1/2}, \tag{2}$$

where I is the intensity of the pump laser, t is the duration of the pump pulse, τ is the lifetime of the upper level of the pumped transition, N_0 is the number of atoms in the lower pumped level, and J is the total angular momentum of the lower pumped level. The factors $\sigma^{\pm}_{JMJ_1M_1}$ are the M-dependent, unsaturated-absorption cross sections for right and left circularly polarized light.

For high intensities, $I > \hbar\omega/2\sigma\tau$, the n_{M_1} saturate, all approaching an M_1-independent value. For such high intensities the rate-equation model is no longer valid, and other processes will become significant. For optimum orientation we must have $I < \hbar\omega/2\sigma\tau$. Assuming that the pump intensity satisfies the above criterion, n_{M_1} is given by

$$n_{M_1} = \frac{N_0}{2J+1}\sum_M \sigma^{\pm}_{JMJ_1M_1}\frac{It}{\hbar\omega}\,. \tag{3}$$

The difference in absorption coefficients for the probe transition is given by

$$\Delta\alpha = \alpha^+ - \alpha^- = \sum_{M_1M_2} n_{M_1}(\sigma^+_{J_1M_1J_2M_2} - \sigma^-_{J_1M_1J_2M_2})\,. \tag{4}$$

Assuming a right circularly polarized pump beam and substituting (3) into (4) yields

$$\alpha^+ - \alpha^- = \frac{N_0 It}{\hbar\omega}\frac{1}{2J+1}\sum_{MM_1M_2}\sigma^+_{JMJ_1M_1}(\sigma^+_{J_1M_1J_2M_2} - \sigma^-_{J_1M_1J_2M_2}). \tag{5}$$

To calculate the photoabsorption cross section, the Born-Oppenheimer approximation will be used for both the initial and final states. In addition, both states are assumed to have zero total spin and belong to Hund's case (a). Under the above conditions, the wave functions for a diatomic molecule are of the form[12]

$$|n\Lambda JM\rangle = |n\Lambda\rangle\left(\frac{2J+1}{8\pi^2}\right)^{1/2}\mathfrak{D}^J_{\Lambda M}(\omega). \tag{6}$$

The $\mathfrak{D}$ functions are the normalized eigenfunctions of a symmetric top and depend on the angular velocities about the body-fixed axes of the molecule.[13] The quantum number Λ is the component of the electronic angular momentum along the internuclear axis, J and M refer to the total angular momentum of the state, and n represents all other quantum numbers which characterize the state. The photoabsorption cross section is proportional to the square of the electric-dipole matrix element given by

$$\langle n'\Lambda'J'M'|T(1q)|n''\Lambda''J''M''\rangle. \tag{7}$$

$T(1q)$ is the dipole operator for right ($q = +1$) and left ($q = -1$) circularly polarized light. The primed variables refer to the final state, and the double primed variables refer to the initial state.

Since a circularly polarized pump laser is being considered, it is best to define the axis of quantization along the direction of propagation of the pump photons. In order to calculate the matrix element in relation (7) with the wave functions of relation (6), the dipole operator must be transformed from the space-fixed coordinate system to the body-fixed coordinate system of the molecule. This transformation is given by Edmonds.[13] The dipole matrix element in relation (7) can then be expressed as

$$\langle n'\Lambda'J'M'|T(1q)|n''\Lambda''J''M''\rangle = (-1)^{\Lambda'-M'}\frac{1}{8\pi^2}[(2J''+1)(2J'+1)]^{1/2} \times\sum_{q'}\langle n'\Lambda'|T(1q')|n''\Lambda''\rangle\int\mathfrak{D}^{J'}_{-\Lambda'-M'}(\omega)\mathfrak{D}^1_{-q'q}(\omega)\mathfrak{D}^{J''}_{\Lambda''M''}(\omega)d\omega. \tag{8}$$

This integral over the $\mathfrak{D}$ functions is evaluated in Ref. 13. Then the photoabsorption cross section can be written as

$$\sigma^q_{J''M''J'M'} = 9\sigma_0(2J''+1)(2J'+1)\begin{pmatrix} J' & 1 & J'' \\ -\Lambda' & \Lambda'-\Lambda'' & \Lambda''\end{pmatrix}^2\begin{pmatrix} J' & 1 & J'' \\ -M' & q & M''\end{pmatrix}^2. \tag{9}$$

Relation (9) is the M-dependent photoabsorption cross section for a diatomic molecule. It has been expressed in a form which is convenient for the evaluation of relative probe intensities, since the total angular-momentum dependence has been written explicitly. All factors which do not depend on the angular momentum are contained in σ_0. If the photoabsorption cross sections in relation (5) are expressed in terms of relation (9), then the difference in absorption coefficients can be simplified to

$$\alpha^+ - \alpha^- = \Delta\alpha_0\frac{1}{(2J+1)(2J_1+1)}S^{\Lambda\Lambda_1}_{JJ_1}S^{\Lambda_1\Lambda_2}_{J_1J_2}\xi^C_{JJ_1J_2}. \tag{10}$$

The S factors are the line strengths or Honl-London factors for the pump and probe transitions, respectively, and are given by (using the convention of Ref. 14)

$$S^{\Lambda''\Lambda'}_{J''J'} = (2J''+1)(2J'+1)\begin{pmatrix} J' & 1 & J'' \\ -\Lambda & \Lambda'-\Lambda'' & \Lambda''\end{pmatrix}^2. \tag{11}$$

The factor $\xi^C_{JJ_1J_2}$ results from the sum over all the M levels and depends on the polarization of the pump laser as well as the angular momenta of the pump and probe transitions. It can be interpreted as a measure of the depolarization experienced by the probe as a result of the orientation in the levels of the pump transition. In the case of a circularly polarized pump laser it is given by

$$\xi^C_{JJ_1J_2} = 9(2J+1)\sum_{MM_1M_2}\begin{pmatrix} J_1 & 1 & J \\ -M_1 & 1 & M\end{pmatrix}^2\left[\begin{pmatrix} J_2 & 1 & J_1 \\ -M_2 & 1 & M_1\end{pmatrix}^2 - \begin{pmatrix} J_2 & 1 & J_1 \\ -M_2 & -1 & M_1\end{pmatrix}^2\right]. \tag{12}$$

For the case of a pump beam linearly polarized at an angle of 45° with respect to the probe beam, Eq. (1)

still gives the probe signal intensity, where $\Delta\alpha$ is now the difference between absorption coefficients parallel and perpendicular to the pump polarization. The same steps are then followed to calculate $\Delta\alpha$ as were used for a circularly polarized pump laser. The difference in absorption coefficients for a linearly polarized pump is given by

$$\alpha^z-\alpha^x=\frac{N_0 It}{\hbar\omega}\frac{1}{2J+1}\sum_{MM_1M_2}\sigma^z_{JMJ_1M_1}(\sigma^z_{J_1M_1J_2M_2}-\sigma^x_{J_1M_1J_2M_2}), \tag{13}$$

where $\sigma^z_{JMJ_1M_1}$ and $\sigma^x_{JMJ_1M_1}$ are the photoabsorption cross sections for polarizations parallel and perpendicular to the pump laser polarization. In this situation, it is best to take the axis of quantization along the direction of the pump laser polarization. Proceeding as before, the difference in absorption coefficients is given by

$$\alpha^z-\alpha^x=\Delta\alpha_0\frac{1}{(2J+1)(2J_1+1)}S^{\Lambda\Lambda_1}_{JJ_1}S^{\Lambda_1\Lambda_2}_{J_1J_2}\zeta^L_{JJ_1J_2}. \tag{14}$$

Here the S factors are the same rotational line strengths that are given by relation (11). The factor $\zeta^L_{JJ_1J_2}$ is the result of the sum over the M levels and is given by

$$\zeta^L_{JJ_1J_2}=9(2J+1)\sum_{MM_1M_2}\begin{pmatrix}J_1&1&J\\-M_1&0&M\end{pmatrix}^2\left\{\begin{pmatrix}J_1&1&J_2\\-M_1&0&M_2\end{pmatrix}^2-\frac{1}{2}\left[\begin{pmatrix}J_1&1&J_2\\-M_1&-1&M_2\end{pmatrix}-\begin{pmatrix}J_1&1&J_2\\-M_1&1&M_2\end{pmatrix}\right]^2\right\}. \tag{15}$$

Combining relations (1) and (10) for a circularly polarized pump beam or (1) and (15) for a linearly polarized pump beam, and neglecting the background term in Eq. (1), the intensity of a probe signal is given by

$$I=I_0\left(\frac{\Delta\alpha_0 l}{4}\right)^2\left(\frac{1}{(2J+1)(2J_1+1)}S^{\Lambda\Lambda_1}_{JJ_1}S^{\Lambda_1\Lambda_2}_{J_1J_2}\zeta^P_{JJ_1J_2}\right)^2, \tag{16}$$

where the superscript P on the ζ factor is given by $P=C$ for a circularly polarized pump beam and $P=L$ for a linearly polarized pump beam. The polarization factors ζ^P, as well as the Honl-London factors, are tabulated in Tables I and II. As an example, the relative probe intensities of a Σ--Π-Δ transition as a function of J are plotted in Fig. 2.

In the limit of large J (>20), the Honl-London and polarization factors simplify to the forms given in Tables III and IV. We can use these large J values in Eq. (16), along with the dipole selection rules to determine the relative intensities obtained with both linearly and circularly-polarized pump beams. In Tables V and VI, these relative intensities, multiplied by 100, are tabulated for

TABLE I. The J dependence of the polarization factor $\zeta^{L_1C}_{JJ_1J_2}$.

$\zeta^C_{JJ_1J_2}$ (circularly polarized pump beam)

	$J_2=J_1+1$	$J_2=J_1$	$J_2=J_1-1$
$J=J_1+1$	$-\frac{3J_1}{2(J_1+1)}$	$\frac{3}{2(J_1+1)}$	$\frac{3}{2}$
$J=J_1$	$\frac{3}{2(J_1+1)}$	$-\frac{3}{2J_1(J_1+1)}$	$-\frac{3}{2J_1}$
$J=J_1-1$	$\frac{3}{2}$	$-\frac{3}{2J_1}$	$-\frac{3(J_1+1)}{2J_1}$

$\zeta^L_{JJ_1J_2}$ (linearly polarized pump beam)

	$J_2=J_1+1$	$J_2=J_1$	$J_2=J_1-1$
$J=J_1+1$	$\frac{3J_1(2J_1-1)}{10(J_1+1)(2J_1+3)}$	$-\frac{3(2J_1-1)}{10(J_1+1)}$	$\frac{3}{10}$
$J=J_1$	$-\frac{3(2J_1-1)}{10(J_1+1)}$	$\frac{3(2J_1+3)(2J_1-1)}{10J_1(J_1+1)}$	$-\frac{3(2J_1+3)}{10J_1}$
$J=J_1-1$	$\frac{3}{10}$	$-\frac{3(2J_1+3)}{10J_1}$	$\frac{3(J_1+1)(2J_1+3)}{10J_1(2J_1-1)}$

TABLE II. Honl-London factors for arbitrary J.

	$S^{\Lambda\Lambda 1}_{JJ_1}$		
	$\Lambda_1=\Lambda+1$	$\Lambda_1=\Lambda$	$\Lambda_1=\Lambda-1$
$J=J_1+1$	$\frac{(J_1-\Lambda_1+1)(J_1-\Lambda_1+2)}{2(J_1+1)}$	$\frac{(J_1+\Lambda_1+1)(J_1-\Lambda_1+1)}{J_1+1}$	$\frac{(J_1+\Lambda_1+2)(J_1+\Lambda_1+1)}{2(J_1+1)}$
$J=J_1$	$\frac{(J_1-\Lambda_1+1)(J_1+\Lambda_1)(2J_1+1)}{2J_1(J_1+1)}$	$\frac{(2J_1+1)\Lambda_1^2}{J_1(J_1+1)}$	$\frac{(J_1+\Lambda_1+1)(J_1-\Lambda_1)(2J_1+1)}{2J_1(J_1+1)}$
$J=J_1-1$	$\frac{(J_1+\Lambda_1-1)(J_1+\Lambda_1)}{2J_1}$	$\frac{(J_1+\Lambda_1)(J_1-\Lambda_1)}{J_1}$	$\frac{(J_1-\Lambda_1-1)(J_1-\Lambda_1)}{2J_1}$

all allowed two-step transitions from a $^1\Sigma_g^+$ ground state. Note that Q-branch transitions are forbidden by parity in a Σ-Σ transition, since the parity of a level of a Σ state depends on J.[15]

Transitions whose intensities are proportional to $1/J^n$ will be too weak to be observed in this high-J limit. Inspection of Tables V and VI then indicates that a two-step signal will be suppressed if a Q-branch transition is pumped with circularly polarized light. Yet, the most intense P- and R-branch probe signals occur if a circularly polarized laser is used to pump a P- or R-branch transition. (An exception to this rule are probe transitions from a $^1\Pi_g$ state to a $^1\Sigma_g^-$ state, which are too weak to observe.) Pumping a P or R branch with circularly polarized light is then useful when searching for new excited states and when collecting data to determine the vibrational and rotational constants for a state, since exposure times can be shorter for these more intense signals. However, a spectrum taken with a circularly polarized pump is useless in determining Λ for an excited state, since the probe spectra taken with a circularly polarized pump laser all exhibit a doublet structure (no Q branches), regardless of the Λ of the excited state. From Table VI we see that once a new state is found, a spectrum taken with a linearly polarized pump beam can be used to determine Λ for that state.

Figure 3 is typical probe spectra taken with linearly and circularly polarized pump light for an $X^1\Sigma_g^+$-$A^1\Sigma_u^+$ pump transition in Na_2. In the first spectrum, taken with a linearly polarized pump laser, the three sets of triplets are three vibrational levels of a highly excited $^1\Pi_g$ state. The doublets in this spectrum are not two-step signals, but result from probe transitions to the $A^1\Sigma_u^+$ state from the lower level of the pumped transition. The spectrum taken with a circularly polarized pump beam consists of doublets for both the $^1\Pi_g$ and the $A^1\Sigma_u^+$ signals. The signals are much more intense here, although the exposure time was actually shorter.

For the calculation done here it was assumed that all of the molecular states were singlet states belonging to Hund's case (a). This is a good approximation for Na_2, which we studied experimentally. In other coupling cases the molecular states can always be described by wave functions whose rotational dependence consists of a linear

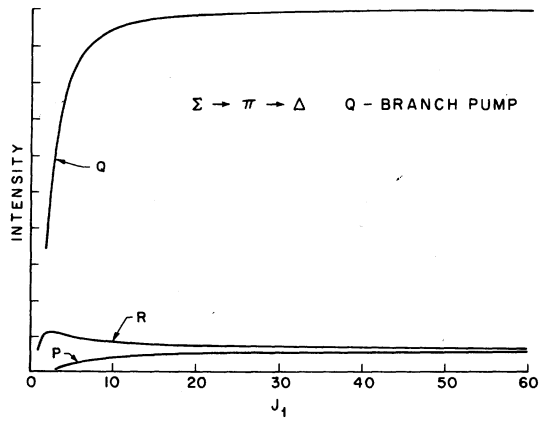

FIG. 2. Intensity of probe signals for a Σ-Π-Δ transition, with a linearly polarized pump. The pumped transition is a Q branch.

TABLE III. Large J values of the Honl-London factors $S^{\Lambda\Lambda 1}_{JJ_1}$.

	$\Lambda_1=\Lambda$	$\Lambda_1=\Lambda\pm1$
$J=J_1+1$	J_1	$\frac{J_1}{2}$
$J=J_1$	$\frac{2\Lambda_1^2}{J_1}$	J_1
$J=J_1-1$	J_1	$\frac{J_1}{2}$

TABLE IV. Large J values of the polarization factors $\zeta^C_{JJ_1J_2}$.

	$\zeta^C_{JJ_1J_2}$		
	$J_2=J_1+1$	$J_2=J_1$	$J_2=J_1-1$
$J=J_1+1$	$-\frac{3}{2}$	$\frac{3}{2J_1}$	$\frac{3}{2}$
$J=J_1$	$\frac{3}{2J_1}$	$-\frac{3}{2J_1^2}$	$-\frac{3}{2J_1}$
$J=J_1-1$	$\frac{3}{2}$	$-\frac{3}{2J_1}$	$-\frac{3}{2}$
	$\zeta^L_{JJ_1J_2}$		
	$J_2=J_1+1$	$J_2=J_1$	$J_2=J_1-1$
$J=J_1+1$	$\frac{3}{10}$	$-\frac{3}{5}$	$\frac{3}{10}$
$J=J_1$	$-\frac{3}{5}$	$\frac{6}{5}$	$-\frac{3}{5}$
$J=J_1-1$	$\frac{3}{10}$	$-\frac{3}{5}$	$\frac{3}{10}$

combination of symmetric top wave functions, all with the same value of J and M. The difference in absorption coefficients $\Delta\alpha$ will have the same form as in relations (10) and (14). The polarization factors ζ will still be given by Eqs. (12) and (15), since these factors depend only on J and M. The rotational line-strength factors will be different, as shown in Ref. 14. Therefore, the formulas developed here can easily be extended to cover any coupling scheme.

TABLE V. Relative intensities for transitions to higher excited states when the pump laser is circularly polarized.

Pumped transition $^1\Sigma_g^+ \rightarrow {}^1\Sigma_u^+$ (P or R branch)		
Excited state	P or R branch	Q branch
$^1\Sigma_g^+$	14	0
$^1\Pi_g$	3.5	$14/J^2$
Pumped transition $^1\Sigma_g^+ \rightarrow {}^1\Pi_u$ (P or R branch)		
Excited state	P or R branch	Q branch
$^1\Sigma_g^+$	0.88	0
$^1\Sigma_g^-$	0	$3.5/J^2$
$^1\Pi_g$	3.5	$14/J^4$
$^1\Delta_g$	0.88	$3.5/J^2$
Pumped transition $^1\Sigma_g^+ \rightarrow {}^1\Pi_u$ (Q branch)		
Excited state	P or R branch	Q branch
$^1\Sigma_g^+$	0	$14/J^4$
$^1\Sigma_g^-$	$3.5/J^2$	0
$^1\Pi_g$	$14/J^2$	$56/J^6$
$^1\Delta_g$	$3.5/J^2$	$14/J^4$

TABLE VI. Relative intensities for transitions to higher excited states when the pump laser is linearly polarized.

Pumped transition $^1\Sigma_g^+ \rightarrow {}^1\Sigma_u^+$ (P or R branch)		
Excited state	P or R branch	Q branch
$^1\Sigma_g^+$	0.56	0
$^1\Pi_g$	0.14	2.3
Pumped transition $^1\Sigma_g^+ \rightarrow {}^1\Pi_u$ (P or R branch)		
Excited state	P or R branch	Q branch
$^1\Sigma_g^+$	0.035	0
$^1\Sigma_g^-$	0	0.56
$^1\Pi_g$	1.4	$2.3/J^2$
$^1\Delta_g$	0.035	0.56
Pumped transition $^1\Sigma_g^+ \rightarrow {}^1\Pi_u$ (Q branch)		
Excited state	P or R branch	Q branch
$^1\Sigma_g^+$	0	9.0
$^1\Sigma_g^-$	0.56	0
$^1\Pi_g$	2.3	$36/J^2$
$^1\Delta_g$	0.56	9.0

III. APPARATUS

A schematic diagram of the two-step polarization-labeling experiment is shown in Fig. 4. The

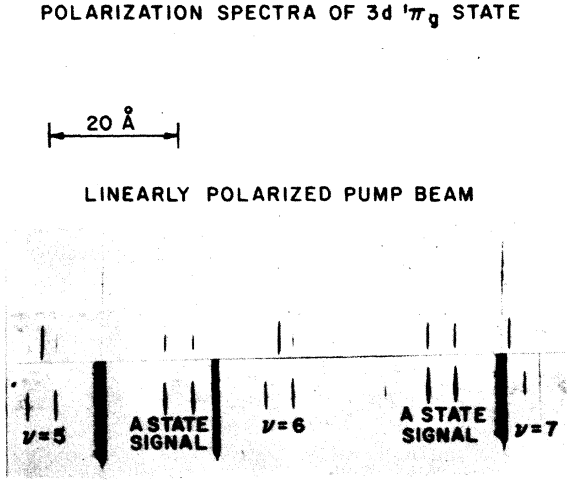

FIG. 3. Polarization spectrum of the $3d\,^1\Pi_g$ state, using both a linearly and a circularly polarized pump beam. The pumped transition is $A(7,28)$–$X(0,27)$.

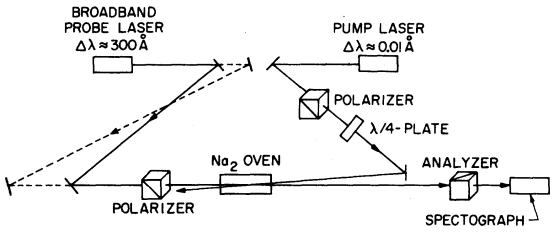

FIG. 4. Schematic of experimental apparatus.

narrow-band pump laser and the broad-band probe laser are pumped by the same Molectron UV 1000 nitrogen laser. The pump beam passes through a linear polarizer and, if circular polarization is desired, a quarter-wave plate. After passing through the polarization optics, the pump beam is reflected off of a mirror and into the sodium oven. The probe beam is polarized at 45° with respect to the pump beam. It travels in the opposite direction from the pump beam through the oven. It is important to make the crossing angle between the pump and probe beams as small as possible, as this will maximize the region of overlap in the sodium oven. Furthermore, the path lengths traveled by both the pump and probe beams must be adjusted so that they counterpropagate in the oven simultaneously. An optical delay line can be introduced to delay the arrival of the probe (dotted line in Fig. 4). After the probe passes through the oven, it is sent through an analyzer. Only those frequencies which have interacted with a level of the pumped transition are transmitted. The probe beam is then sent through a spectrograph, and the spectrum of the probe frequencies is recorded on film.

The narrow-band dye laser is of the Hänsch design.[16] A 3.5-mm air-spaced etalon is placed in the laser cavity to obtain a narrow-bandwidth (1 GHz). The grating and etalon are enclosed in a vacuum can to allow pressure tuning.[17] The output of the oscillator is amplified by passing it through a second side-pumped dye cell which acts as a single-stage traveling-wave amplifier. Depending on the dye used, this results in a peak power of 1 to 10 kW, which is usually attenuated using neutral-density filters. The duration of the pulse is 5 nsec. A loose focus of the pump beam is used so that its waist is about 5 mm throughout the active region of the oven. This large spot size facilitates overlap with the probe beam inside the oven.

The broad-band probe laser consists of a single side-pumped dye cell with the superfluorescent spot reflected back through the active region. Laser action occurs over the entire gain profile of the dye, resulting in a 100 to 300 Å bandwidth. The probe beam is focused so that its waist is about 5-mm in the active region of the oven. The variety of commercially available dyes for the probe laser covers the visible region of the electromagnetic spectrum (4000–7500 Å).[18]

The sodium oven consists of a 70-cm-long, stainless steel pipe with a clam shell oven fitted over the middle 30 cm. Near each end of the clam shell oven, water-cooled blocks are attached to the pipe to keep the sodium away from the windows. Typically the sodium is heated to a temperature of 450 °C. This corresponds to a Na pressure of about 1 torr and a Na_2 pressure of about 20 μm.[19] The choice of windows is very important, since background birefringence must be minimized. It is necessary to use a material which has a very low birefringence while under stress. We have found the $\frac{1}{4}$-inch-thick SF57 glass made by Schott Optical Company very suitable for this purpose. Using these windows and Glan-Thompson polarizers, extinction ratios of less than 10^{-6} are obtained.

IV. EXPERIMENTAL PROCEDURE

Using the constants of Kusch and Hessel,[20,21] we have calculated the wavelength and intensity of X–A and X–B transitions.[22] From this list a strong transition with the desired upper-state rotational and vibrational quantum numbers is chosen. The pump laser is tuned to within an angstrom of the desired transition. By slowly pressure tuning the pump laser while monitoring the intensity transmitted by the oven, an absorption spectrum is generated. We then tune the pump to one of the strong absorption signals and take a polarization spectrum with the probe containing the same dye as the pump. The resulting spectrum shows strong signals from the oriented level in the X state to the A or B state, including the pumped transition. From this spectrum and the known rotational constant of the A or B state, we can easily determine the type (P, Q, or R) and J value of the pumped transition. Repeating this process for several of the strong lines appearing on the absorption scan, we can match up the calculated and observed transitions to determine which is the desired pump line.

Before taking a polarization spectrum, it is important to optimize the pump and probe intensities. It is desirable to have the broad-band probe as bright as possible without the appearance of mode structure. To achieve this, the light from the nitrogen laser is focused rather loosely into the probe dye cell. The optimal pump intensity is slightly less than the saturation intensity of the transition. As was discussed in Sec. II, at high intensities our theory is no longer valid since the

rate-equation model breaks down; however, the pump must be strong enough to populate the intermediate level. Depending on the wavelength of the pump and the transition pumped, neutral-density filters are sometimes used to attenuate the pump.

To take a polarization spectrum we pressure scan the frequency of the pump laser to the peak of the desired transition. (The frequency of the laser will drift less than 1 GHz in an hour.) The pump and probe overlap in the oven is then maximized, since good overlap over the entire active region is essential. The probe spectra are recorded using a 3-m Bausch and Lomb spectrograph with 1800 lines/mm grating. The dispersion is about 2 Å/mm. Three types of 4 × 5-inch sheet films are used to record the spectra. For probes with wavelengths longer than 6500 Å, Kodak High Speed Infrared Film is used. For shorter wavelengths, either Kodak Royal Pan (ASA 400) or Kodak Royal X Pan (ASA 1200) is used. Exposure times vary between 10 and 30 minutes, depending on the expected intensity of the signals. In order to determine the wavelength of the probe signals, the spectrum from a neon lamp is recorded with the probe signals. For wavelengths greater than 6500 Å an iodine spectrum is also used. A Grant Comparator is used to measure the positions of the probe signals and the reference lines on the sheet film.

A quadratic fit is used to determine the wavelengths of the probe signals. The energy of the new excited level relative to the bottom of the $X\,^1\Sigma_g^+$ state is then calculated by adding together the energy of the probe transition, the energy of the pumped transition, and the energy of the lower level of the pumped transition. The lower-level energy is calculated using the constants of Refs. 20 and 21.

The various types of signals that occur are indicated in Fig. 5.[1] Type 2 is the desired two-step

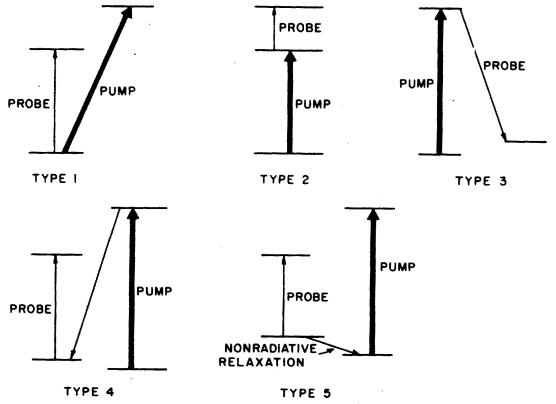

FIG. 5. Types of probe signals occurring in polarization labeling.

polarization labeling where oriented molecules are produced in an intermediate state and absorption lines to higher electronic states are obtained. The other types of signals are easy to distinguish from two-step polarization labeling. Type 1 signals will exhibit the rotational and vibrational structure of the upper level of the pumped transition, while type 3 signals will exhibit structure of the lower level of the pumped transition. Since the constants for these states are known for Na_2, these signals can easily be identified and eliminated. Furthermore, as mentioned earlier, these signals can be used to assign vibrational and rotational quantum numbers to the levels of the pumped transition. Since a pulsed pump and probe laser are used, two-step polarization-labeling signals do not occur when the probe is delayed for a time longer than the lifetime of the intermediate state. Thus, one can distinguish between type 1 and 2 signals even if the constants for the intermediate level are not well known. The type 4 and 5 signals are usually not seen. However, they can easily be identified when they do occur. Type 4 signals will be observed to increase as the delay time between the pump and probe laser is increased. These signals will exhibit the rotational and vibrational structure of the upper level of the pumped transition. The type 5 signals will not occur unless the collisional transfer rate from levels of the pumped transition to nearby levels is faster than the radiative decay rate. When such collisions occur, the rotational quantum number of the pumped levels can only change by an even number and the induced optical anisotropy is preserved.[11,23] Usually type 5 signals are not observed unless a buffer gas is present in the sample.

V. EXCITED STATES IN DIATOMIC SODIUM

Six *ungerade* states in Na_2 are known from absorption spectroscopy.[24] The A, B, and X states have been thoroughly studied.[20,21] Using two-step polarization labeling we have identified 24 excited *gerade* states. The classifications and electronic energies are shown in Fig. 6. The $^1\Delta_g$ states are the low-lying members of a molecular Rydberg series, while the $^1\Pi_g$ states span the transition from molecular states to Rydberg states.

We have summarized our results in terms of a Dunham expansion:

$$T(v)=\sum_{i,j} Y_{ij}(v+\tfrac{1}{2})^i[J(J+1)-\Lambda^2]^j . \qquad (17)$$

Unfortunately the values of the coefficients depend on the range of v and J that is fit, as well as on the number of coefficients included. Therefore, we have restricted our fit to a standard range (0

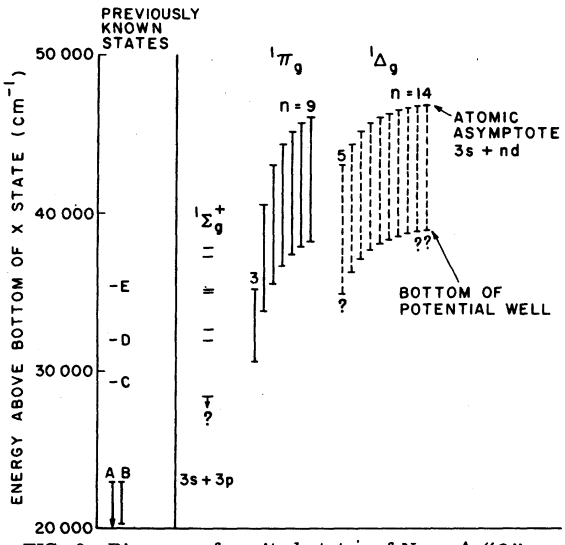

FIG. 6. Diagram of excited states of Na_2. A "?" indicates that the bottom of the potential well is uncertain. For all of the $^1\Sigma_g^+$ states, the plotted line represents the lowest observed vibrational band. See Table VIII for details.

$\leq \nu \leq 7$ for $^1\Pi_g$ states, $0 \leq \nu \leq 3$ for $^1\Delta_g$ states, and $19 \leq J \leq 41$ for both) and a standard set of five coefficients. For the 13 states for which we have enough points to provide reasonably uniform coverage of this range, the fitted constants are presented in Table VII. After removing a few deviant points, we find that the estimated error of the fit is 0.3 to 0.4 cm^{-1}, in agreement with the uncertainty in making a single measurement. We find no systematic deviations from the five-parameter fit within this restricted range.

We have estimated the size of Y_{30} and Y_{02} by fitting to points outside the restricted range. For the $4d\pi$ state we have a few points at $J \sim 70$. They suggest the addition of a $Y_{02} = -0.5 \times 10^{-6}$ term with an increase of the Y_{01} term by ~0.001. For the $3d\pi$ state we have vibrational levels up to $\nu = 26$. Including these levels gives essentially the same values for the five standard constants if a $Y_{30} = -0.7 \times 10^{-3}$ term is added. These values for Y_{02} and Y_{30} are small enough that they should produce no systematic deviation in the fit of our data to the Dunham expansion using the five standard constants in our restricted range. Moreover, these values for Y_{02} and Y_{30} are similar to those found for these constants in the X, A, and B states.[22]

In the absence of any direct observations we have assigned asymptotes to the states by indirect arguments. The ground state of Na_2 has the configuration $KKLL(3s\sigma_g)^2$, the A state is $KKLL(3s\sigma_g)(3p\sigma_u)$, and the B state is $KKLL(3s\sigma_g)(3p\pi_u)$. The strongest molecular transitions are expected to be those corresponding to the allowed atomic transitions. Thus the singly excited states observed in transitions from the A or B states are $3s+ns$ or $3s+nd$. Transitions to doubly excited states, $3p+np$ are also allowed; however, only the $3p+3p$ configurations are low enough in energy to have been seen in this experiment.

The $^1\Delta_g$ states and the $^1\Pi_g$ states form the beginnings of two molecular Rydberg series,[4] corresponding to the $3s+nd$ asymptotes. The $^1\Delta_g$ states

TABLE VII. Constants for the well-characterized $^1\Delta_g$ and $^1\Pi_g$ states. All constants are given in units of cm^{-1}. The seemingly superfluous digits are necessary to compensate for the effects of correlations between the constants.

n	Points	σ	Y_{00} (σ_{00})	Y_{10} (σ_{10})	Y_{01} ($\sigma_{01}\times10^3$)	Y_{20} (σ_{20})	$Y_{11}\times10^3$ ($\sigma_{11}\times10^3$)
$^1\Delta_g$ states							
6	55	0.22	36 250.68 (0.2)	121.014 (0.1)	0.113 86 (0.1)	−0.4185 (0.03)	−0.662 (0.06)
7	75	0.30	37 100.77 (0.2)	119.741 (0.2)	0.112 80 (0.2)	−0.3704 (0.04)	−0.402 (0.08)
8	85	0.26	37 659.54 (0.2)	120.217 (0.1)	0.113 33 (0.2)	−0.4334 (0.03)	−0.736 (0.07)
9	96	0.28	38 047.18 (0.2)	120.221 (0.1)	0.112 85 (0.2)	−0.4510 (0.03)	−0.740 (0.07)
10	70	0.31	38 325.71 (0.2)	119.917 (0.2)	0.112 66 (0.2)	−0.3599 (0.04)	−0.638 (0.09)
11	52	0.46	38 531.80 (0.3)	120.122 (0.3)	0.112 79 (0.3)	−0.3442 (0.09)	−1.205 (0.19)
12	31	0.29	38 688.94 (0.3)	119.489 (0.3)	0.112 36 (0.3)	−0.2633 (0.09)	−0.563 (0.30)
$^1\Pi_g$ states							
3	57	0.31	30 582.73 (0.3)	102.579 (0.1)	0.103 05 (0.4)	−0.3549 (0.01)	−0.573 (0.08)
4	65	0.40	33 810.66 (0.3)	107.590 (0.1)	0.104 26 (0.6)	−0.4724 (0.02)	−0.344 (0.12)
5	52	0.30	35 550.77 (0.3)	112.128 (0.1)	0.107 19 (0.2)	−0.5112 (0.01)	−0.541 (0.05)
6	85	0.26	36 634.01 (0.1)	115.560 (0.1)	0.109 39 (0.1)	−0.4746 (0.01)	−0.601 (0.04)
7	128	0.36	37 344.74 (0.2)	117.668 (0.1)	0.111 13 (0.3)	−0.4809 (0.01)	−0.568 (0.05)
8	96	0.45	37 828.69 (0.3)	118.527 (0.2)	0.112 47 (0.2)	−0.4338 (0.03)	−0.527 (0.10)
9[a]	30	0.49	38 169.33 (0.4)	119.96 (0.4)	0.112 63 (0.4)	−0.6826 (0.06)	−0.238 (0.23)

[a] Only levels up to $\nu = 4$ used to fit this state.

correspond to a $KKL(3s\sigma_g)(nd\delta_g)$ configuration for $n=5$ to 14, while the $^1\Pi_g$ states correspond to $KKLL(3s\sigma_g)(nd\pi_g)$ for $n=3$ to 9. To make this identification, we matched the differences in electronic energies, $T_0(n)$, between adjacent states in a series to the differences in energies between adjacent $3s+nd$ asymptotes. We assume that for these states the potential well depths are roughly constant. This is reasonable since here the Na_2 molecule consists of an Na_2^+ core and an nd electron far away from this core, which does not contribute significantly to the molecular bond.

We can calculate the dissociation energies of these states by adding the depth of the X state[20] to the energy of the $3s+nd$ asymptote[25] and substracting from this the electronic energy T_0 of the corresponding electronic state. We plot D versus $1/n^2$ for both series in Fig. 7. (We use $1/n^2$ since the radius of a Rydberg orbit scales roughly as n^2, and the electronic energy has a hydrogenic $1/n^2$ dependence.) For large n the dissociation energy changes only slightly with n, as assumed. Both series approach approximately the same value in the large-n limit, which corresponds to the dissociation energy of the $KKLL(3s\sigma_g)\ ^2\Sigma_g^+$ ground state of Na_2^+. The dissociation energy for Na_2^+ lies between the large n values of this quantity for the $^1\Pi_g$ and $^1\Delta_g$ series, which is 7950 cm^{-1} to within about 50 cm^{-1} (Ref. 26). This value is consistent with the results of previous experimental[27-29] and theoretical[30-32] studies. (Although for a given state the dissociation energy depends on the asymptote assignment, the extrapolated value is independent of it, since for large n the asymptote energies approach a constant value, the ionization limit of Na_2.) The n dependence of the dissociation energy provides a check on the assignment of asymptotes for these states. In the $^1\Delta_g$ series, the excited electron is a bonding electron. For small values of n this electron lives close to the Na_2^+ core, and its bonding effect is felt, resulting in a deep potential well. As n increases this electron is removed from the vicinity of the core and the molecule becomes less deeply bound. Eventually this electron has no effect on the molecule, and the dissociation energy approaches a constant. This behavior is indeed seen in the $^1\Delta_g$ Rydberg series. In the $^1\Pi_g$ series the excited electron is antibonding, and the opposite behavior is seen, as expected. For a given n, the molecular orbital for an $nd\pi_g$ electron penetrates the Na_2^+ core more than an orbital for an $nd\delta_g$ electron. The dissociation energy for a $^1\Pi_g$ state should deviate more from the value of Na_2^+ than the dissociation energy of the corresponding $^1\Delta_g$ state. This behavior is clearly seen in Fig. 7, again indicating that our identification is correct.

In Figs. 8 and 9 we exhibit the n dependence of

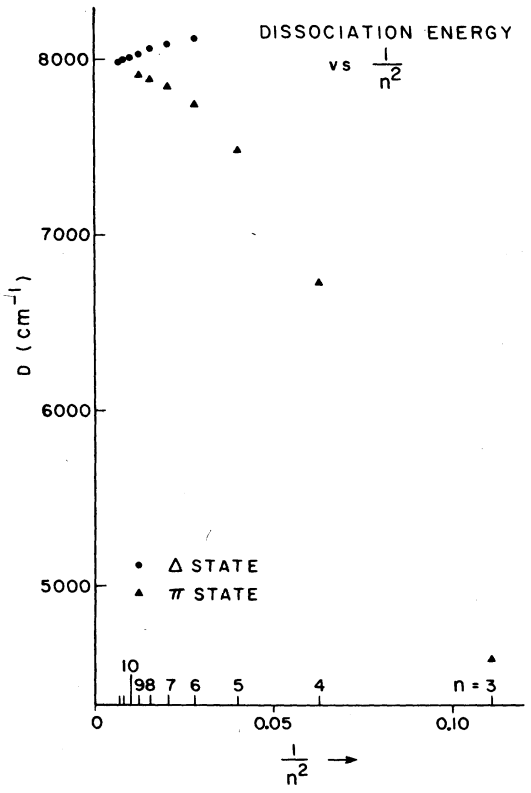

FIG. 7. Dissociation energy (D), using the asymptote assignment shown in Fig. 6, as a function of $1/n^2$.

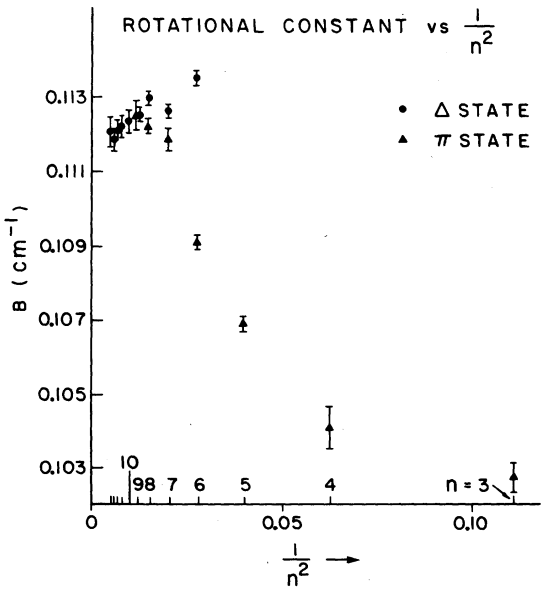

FIG. 8. Rotational constant, as defined in Eq. (18), as a function of $1/n^2$.

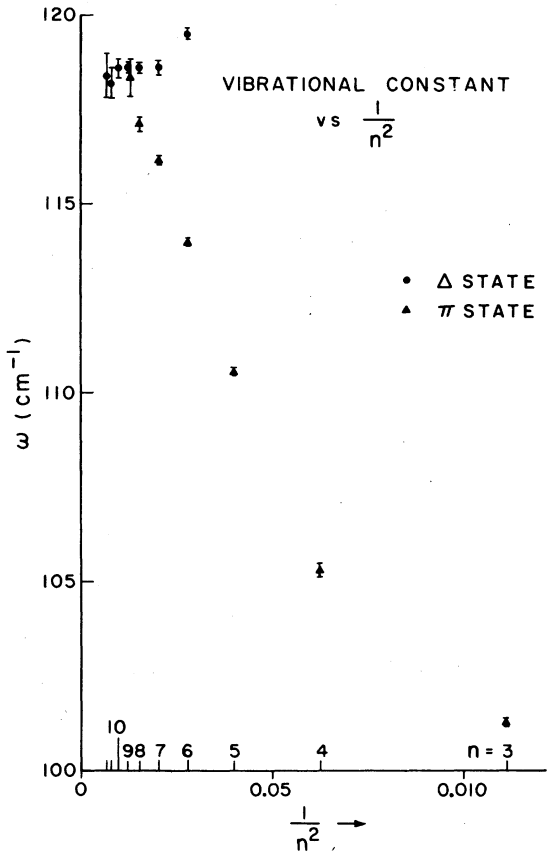

FIG. 9. Vibrational constant, as defined in Eq. (19), as a function of $1/n^2$.

the rotational and vibrational constants. To avoid the uncertainties of extrapolating, as well as the effects of correlations between the constants, we do not plot the fitted constants themselves, but rather the combinations

$$B = Y_{01} + 0.5Y_{11}, \tag{18}$$

$$\omega = Y_{10} + 1000Y_{11} + 2Y_{20}. \tag{19}$$

B is the effective rotational constant in the $v=0$ band (in the region $19 \leq J \leq 41$ where the constants are fitted), while ω is the difference in energy between the $v=0$ and $v=1$ bands at $J \sim 31$. The rotational and vibrational constants in the $^1\Delta_g$ and the $^1\Pi_g$ series become equal at $n=9$. The vibrational constant increases with increasing n for the $^1\Pi_g$ states, since the antibonding electron is interacting less with the core, strengthening the molecular bond. As expected the $^1\Delta_g$ states exhibit a much less marked decrease in ω with increasing n. The rotational constant increases with increasing n for the $^1\Pi_g$ states, indicating that the bond length is decreasing with increasing n. Again the molecular bond is becoming stronger as n increases. For the $^1\Delta_g$ series, the rotational constant shows only a slight decrease with increasing n. We can extrapolate to $n=\infty$ to estimate the rotational and vibrational constants of Na_2^+. For the vibrational constant all of the large n values are within 0.5 cm^{-1} of 119 cm^{-1}. For the rotational constant all large n values are within 0.0005 cm^{-1} of 0.112 cm^{-1}. So, to within a few percent, the extrapolated values of these constants are $\omega = 119$ cm^{-1} and $B = 0.112$ cm^{-1}. These values are consistent with previous theoretical calculations.[32,33]

None of our $^1\Delta_g$ or $^1\Pi_g$ states can be identified with the doubly excited $3p+3p$ configuration for the following reasons. The $3p\sigma_u$ orbital is antibonding, while the $3p\pi_u$ orbital is bonding. A doubly excited $^1\Pi_g$ state would correspond to the configuration $KKLL(3p\sigma_u)(3p\pi_u)$, and so would be unbound or weakly bound, while a $^1\Delta_g$ state would correspond to $KKLL(3p\pi_u)(3p\pi_u)$ and would be weakly bound. Since the $3p+3p$ asymptote lies at 39 902 cm^{-1}, one would expect to find these states at energies above 35 000 cm^{-1}. As discussed previously, all of the $^1\Pi_g$ and $^1\Delta_g$ states in this region fit well with the $3s+nd$ series. This fact is especially apparent when one looks at the constants for these states (Figs. 7, 8, and 9). One would expect a doubly excited state to exhibit radically different behavior than a singly excited one, yet all of these states have similar properties.

For $n \sim 12$, the vibrational spacing becomes smaller than the spacing between adjacent electronic states. In this case one should view these excited states as consisting of a series of electronic levels for each vibrational band, rather than the usual view of vibrational structure superimposed on each electronic state. Figure 10 illustrates this point. In this polarization spectrum we see the $v=7$ vibrational band of the three highest $^1\Pi_g$ states ($n=7,8,9$), rather than a typical spectrum of several vibrational bands of a single state, as in Fig. 3.

In addition to the seven well-characterized $^1\Delta_g$ states we have three others for which we can provide preliminary constants. For the $13d\delta_g$ and $14d\delta_g$ states we have only one vibrational band, believed to be the $v=0$ band. For the $5d\delta_g$ state we have two consecutive bands, but we may not have seen the $v=0$ band. Table VIII summarizes the known properties of these states.

We have also discovered and partially characterized seven $^1\Sigma_g^+$ states. Preliminary constants are given in Table VIII. We probably have not seen the lowest vibrational band for any of these states; we tentatively identify the lowest band seen as the $v=1$ band in all but the lowest state.

In this region there are two kinds of singly excited $^1\Sigma_g^+$ states that have allowed transitions from the A and B states, namely, those with configura-

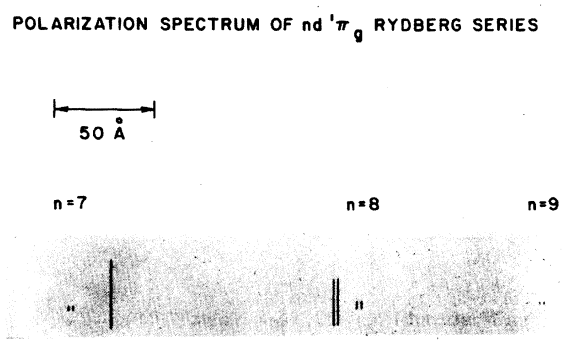

FIG. 10. Polarization spectrum of the $nd\,^1\Pi_g$ Rydberg series. The $v=7$ vibrational bands of the $n=7$, 8, and 9 $^1\Pi_g$ Rydberg states are shown. The pumped transition is $A\,(7,28)-(0,27)$.

tions $KKLL(3s\sigma_g)(nd\sigma_g)$ and those with $KKLL(3s\sigma_g) \times (ns\sigma_g)$. The lowest three states we tentatively assign to $3s+3d$, $3s+5s$, and $3s+4d$ asymptotes. The next two states probably correspond to $3s+6s$ and $3s+5d$, although the order is not clear.

Currently, the longest wavelength we can attain with our system is 7500 Å, which corresponds to a minimum energy of 28 100 cm^{-1} while pumping the A state and 33 700 cm^{-1} while pumping the B state. Since transitions to $^1\Pi_g$ states can occur from either the A or B states, we have been able to follow that series from the beginning. Transitions to $^1\Delta_g$ states are only allowed from the B state, so we have not seen the $n=3$ or $n=4$ $^1\Delta_g$ states. The $3s+4s\,^1\Sigma_g^+$ state and the bottom of the $3s+3d\,^1\Sigma_g^+$ states are also out of our reach. Extending the wavelength range would allow us to study the transition from molecular to Rydberg behavior in the $^1\Sigma_g^+$ and $^1\Delta_g$ series.

Even though it was possible to probe continuously up to and above the ionization limit, no signals were seen above $n=14$. Presumably this results from the weak transition rate to large n orbits ($1/n^3$ dependence). A thermionic diode would provide a more sensitive detector for these Rydberg states.[34]

VI. CONCLUSION

Two-step polarization labeling has proven to be a simple and effective method for surveying large sections of the spectrum of Na_2. With improvements in detection efficiency, the $^1\Sigma_g^+$ states and higher-lying Rydberg levels should be accessible. Even without refinement the technique could yield interesting results for other molecules.

TABLE VIII. Preliminary constants for the $n=5$, 13, and 14 $^1\Delta_g$ states and the $^1\Sigma_g^+$ states. All constants are given in units of cm^{-1}. B is the rotational constant of the lowest observed vibrational band, while T_0 is the energy of the bottom of this band. ω is the vibrational spacing between the two lowest levels for $J\sim 31$. These constants reproduce the observed signals in these bands to within 0.5 cm^{-1}.

$^1\Delta_g$ states							
	$5d\delta_g$		$13d\delta_g$		$14d\delta_g$		
B	0.1133		0.1118		0.1121		
ω	121.3						
T_0	34 935.4		38 870.4		38 966.7		
$^1\Sigma_g^+$ states							
B	0.0887	0.1078	0.1056	0.1080	0.1102	0.1124	0.1112
ω	107.6	109.1	121.5	113.7	116.1		
T_0	28 380.5	31 937.3	32 623.8	34 997.2	35 154.9	37 225.3	37 815.1
Number of vibrational bands seen	29	17	19	3	5	1	1

ACKNOWLEDGMENTS

We would like to thank Professor T. W. Hänsch and Professor R. N. Zare for many helpful discussions. We would also like to thank Frans Alkemade and Ken Sherwin for their skilled technical assistance. One of us (A.J.T.), gratefully acknowledges the support of the John and Fannie Hertz Foundation. This work was supported by the National Science Foundation under Grant No. PHY80-10689.

---

*Present address: Bell Laboratories, Murray Hill, New Jersey.

[1]M. E. Kaminsky, R. T. Hawkins, F. V. Kowalski, and A. L. Schawlow, Phys. Rev. Lett. 37, 683 (1976).

[2]R. E. Teets, R. Feinberg, T. W. Hänsch, and A. L. Schawlow, Phys. Rev. Lett. 37, 683 (1976).

[3]N. W. Carlson, F. V. Kowalski, R. E. Teets, and A. L. Schawlow, Opt. Commun. 29, 302 (1979). (Note that the vibrational assignment of the $^1\Pi_g$ has been changed. Vibrational quantum numbers for this state were reassigned by looking for a sharp cutoff of two-step signals toward the red when the $v=1$ vibrational level of the A state was pumped.)

[4]N. W. Carlson, A. J. Taylor, and A. L. Schawlow, Phys. Rev. Lett. 45, 18 (1980). (The n assignment for the $^1\Pi_g$ and the $^1\Delta_g$ states has been changed.)

[5]N. W. Carlson, Ph.D. thesis (Stanford University, (1980), G. L. Report No. 3114 (unpublished).

[6]J. P. Woerdman, Chem. Phys. Lett. 43, 279 (1976).

[7]R. Vasuedev, T. M. Stachelek, and W. M. McClain, Opt. Commun. (in press).

[8]R. A. Bernheim, L. P. Gold, P. B. Kelly, C. Kittrell, and D. K. Veirs, Phys. Rev. Lett. 43, 123 (1979).

[9]R. A. Bernheim, L. P. Gold, P. B. Kelly, T. Tipton, and D. K. Veirs, J. Chem. Phys. 74, 2749 (1981).

[10]*Laser Polarization Spectroscopy*, in Proceedings of SPIE Conference on Advances of Laser Spectroscopy I, August 23–24, 1977 (SPIE, Bellingham, 1977), Vol. 113, p. 80.

[11]R. E. Teets, Ph.D. thesis (Stanford University, 1978), G. L. Report No. 2821 (unpublished).

[12]L. D. Landau and E. M. Lifshitz, *Quantum Mechanics* (Pergamon, New York, 1976).

[13]A. R. Edmonds, *Angular Momentum in Quantum Mechanics* (Princeton University Press, Princeton, New Jersey, 1974).

[14]R. N. Zare, in *Molecular Spectroscopy: Modern Research* (Academic, New York, 1974), pp. 207–221.

[15]G. Herzberg, in *Molecular Spectra and Molecular Structure:* Vol. 1, *Spectra of Diatomic Molecules* (Van Nostrand Reinhold, New York, 1950).

[16]T. W. Hansch, Appl. Opt. 11, 895 (1972).

[17]R. Wallenstein and T. W. Hänsch, Appl. Opt. 13, 1625 (1974).

[18]Exciton Laser Dyes, Exciton Chemical Company, Dayton, Ohio.

[19]M. Lapp and L. P. Harris, J. Quant. Spectrosc. Radiat. Transfer 6, 169 (1966).

[20]P. Kusch and M. M. Hessel, J. Chem. Phys. 68, 2591 (1978).

[21]P. Kusch and M. M. Hessel (unpublished).

[22]M. E. Kaminsky, Ph.D. thesis (Stanford University, 1976), G. L. Report No. 2531 (unpublished).

[23]R. E. Drullinger and R. N. Zare, J. Chem. Phys. 59, 4225 (1973).

[24]S. P. Sinha, Proc. Phys. Soc. London 59, 610 (1947).

[25]C. E. Moore, *Atomic Energy Levels*, Nat'l. Bur. Stds. (U. S.) Circ. No. 467 Circular of the N. B. S. (1949) (U. S. GPO, Washington, D. C., 1957.)

[26]S. Leutwyler, M. Hofmann, H. P. Harri, and E. Schumacher, Chem. Phys. Lett. 77, 257 (1981). This Letter, which appeared after this manuscript was submitted, gives $D=7920$ cm^{-1} for Na_2^+, in extremely good agreement with our value of 7950 cm^{-1}.

[27]R. D. Hudson, J. Chem. Phys. 43, 1790 (1965).

[28]R. F. Barrow, N. Travis, and C. V. Wright, Nature (London) 187, 141 (1960).

[29]This is equivalent to an ionization energy of 39 490 cm^{-1}, which can be derived from a simple thermodynamic cycle, using the X state dissociation energy of Ref. 20.

[30]C. J. Cerjan, K. K. Docken, and A. Dalgarno, Chem. Phys. Lett. 38, 401 (1976).

[31]D. D. Konowalow and M. E. Rosenkrantz (private communication).

[32]J. N. Bardsley, B. R. Junker, and D. W. Norcross, Chem. Phys. Lett. 37, 502 (1976).

[33]P. J. Bertoncini and A. C. Wahl (unpublished).

[34]L. R. Pendrill, D. Delande, and J. C. Gay, J. Phys. B 12, L603 (1979).

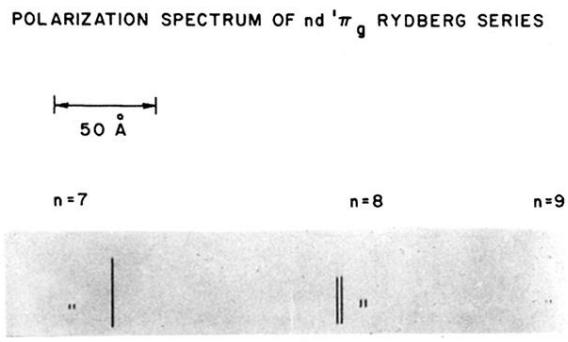

FIG. 10. Polarization spectrum of the $nd\,^1\Pi_g$ Rydberg series. The $v=7$ vibrational bands of the $n=7$, 8, and 9 $^1\Pi_g$ Rydberg states are shown. The pumped transition is $A\,(7,28)-(0,27)$.

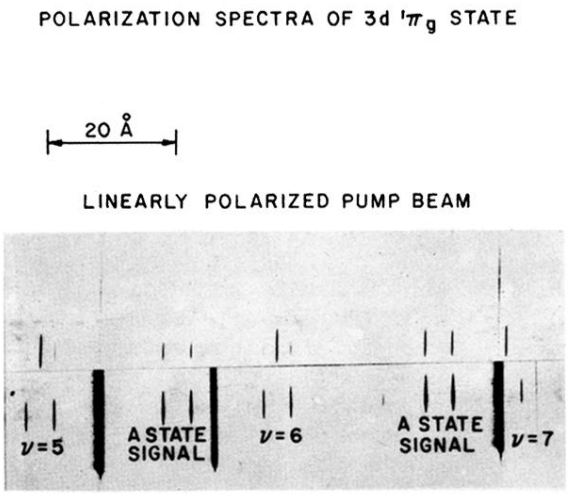

FIG. 3. Polarization spectrum of the $3d\,^1\Pi_g$ state, using both a linearly and a circularly polarized pump beam. The pumped transition is $A(7,28)$–$X(0,27)$.